

A. T. Pathan<sup>1</sup>, A. M. Shaikh<sup>2</sup>, S.K.Sushant<sup>3</sup>, Shridhar N. Mathad<sup>3\*</sup>

## Effect of synthesis methods and comparative study of structural properties of micro and nano Ferrites

<sup>1</sup>Department of Physics, M.H. SabooSiddik College of Engineering, Mumbai, 400008, India, [asrar.pathan@rediffmail.com](mailto:asrar.pathan@rediffmail.com).

<sup>2</sup>Department of Electronics, The New College, Kolhapur, 416014, India

<sup>3</sup>Department of Engineering Physics, K.L.E. Institute of Technology, Gokul Road, Hubballi, 580027 Karnataka, India

[physicssiddu@gmail.com](mailto:physicssiddu@gmail.com), [physicssiddu@kleit.ac.in](mailto:physicssiddu@kleit.ac.in)

In this study,  $Mn_xZn_{(1-x)}Fe_2O_4$  ferrite samples with  $x = 0.4$  and  $0.6$  were synthesized using a solid-state method and co-precipitation method. In order to determine the effects of various concentrations ( $x$ ) on the ferrite's structure, particle size, and crystalline phases, prepared samples were analyzed using X-ray diffraction (XRD). The XRD patterns revealed that the synthesized samples display a single-phase cubic spinel structure. FTIR analysis showed for both synthesis method have absorption band in the range 400 to 1000  $cm^{-1}$ . SEM analysis shows extreme homogeneity of all the samples. EDX analysis was used to examine for  $Mn_{0.4}Zn_{0.6}Fe_2O_4$ . The prepared ferrites powders contain Mn, Zn, and Fe, as shown in both synthesis methods. In this approach, alternative synthesis routes for these ferrites are suggested in this study in order to get around some limitations of the traditional preparation method.

**Keywords:** Ferrites, XRD, Solid state method, co-precipitation method.

Received 14 January 2023; Accepted 8 March 2023.

### Introduction

Ferrites are a class of substances that have attracted a lot of attention recently because of their magnetic [1] and electrical characteristics [2,3], which make them perfect for a variety of applications in industries including electrical engineering, electronics, and tele communications [4,5]. Ferrites have been extensively used as magnetic cores in transformers, inductors, and other electrical components, and have been the subject of many studies due to their potential applications in magnetic data storage, microwave devices, and biomedical engineering. The properties of ferrites can be tailored by controlling the synthesis methods and particle size. In this context, micro and nano-sized ferrites have become increasingly popular due to their unique properties that differ from their bulk counterparts. The small particle size of micro and nano ferrites results in high surface-to-volume ratios, leading to enhanced

magnetic and electrical properties, as well as increased reactivity. The synthesis method used to produce ferrites has a significant impact on the structural and magnetic properties of the resulting material. For example, the synthesis process can determine the particle size, crystalline structure, and magnetic properties of ferrites [6-8]. Solid-state and solution-based approaches are the two primary groups into which ferrites' synthesis techniques may be divided. Solid-state methods, such as ceramic and sintering processes, produce ferrites with a dense and homogeneous structure, while solution-based methods, such as sol-gel, precipitation, and co-precipitation, produce ferrites with a more porous structure [9,10].

In this study, we aim to provide a comprehensive introduction to the effect of synthesis methods on the structural properties of ferrites and a comparative study of the structural properties of micro and nano ferrites [11,12]. The study will focus on the synthesis methods used to produce ferrites and the resulting structural properties,

including particle size, crystalline structure, and magnetic properties. The article will begin by providing an overview of the different synthesis methods used to produce ferrites, including solid-state and solution-based methods. The impact of various synthesis techniques on the crystalline structure, magnetic properties, and particle size of ferrites will thereafter be the main topic of discussion [13]. The structural characteristics of micro and nano ferrites will next be compared, with a focus on the variations in particle size, crystalline structure, and magnetic properties between these two categories of ferrites.

In conclusion, this article will provide a comprehensive overview of the effect of synthesis methods and a comparative study of the structural properties of micro and nano ferrites. By understanding the relationship between synthesis methods and structural properties, it is possible to optimize the synthesis process and tailor the properties of ferrites for specific applications [14,15].  $Mn_xZn_{(1-x)}Fe_2O_4$  Co-precipitation and ceramic methods have been used to synthesis ferrites [10,16,17]. The physical and structural, of these samples have been investigated and the final ferrite product has been identified using established analytical and experimental techniques.

## I. Experimental

### Samples preparation:

#### A. Wet-chemical method (co-precipitation method):

Wet chemical (co-precipitation approach) procedure were used to create manganese zinc ferrites from the series of  $Mn_xZn_{(1-x)}Fe_2O_4$  ( $x = 0.4, \text{ and } 0.6$ ). The Schematic diagram of co-precipitation method shown in fig 1. NaOH and  $FeCl_3$  concentrations for each sample were held constant. Fe:Na ratios were obtained at a 1:4 ratio for each sample. For each sample, varying amounts of the salts

$MnCl_2 \cdot 4H_2O$ ,  $ZnCl_2$ , and  $FeCl_3$  were dissolved in distilled and deionized water. NaOH solution in a 100 ml beaker was stirred at room temperature using a magnetic stirrer at a speed of 60rpm. Drop by drop, the metallic ion solution was poured into the beaker holding the NaOH solution. Dark grey precipitates were produced during addition. The beaker containing the dark grey precipitates was set into a bath of water and ethylene glycol that had been preheated. Each sample received a different water bath temperature 60 minutes were spent on. After 60 minutes, the particles finally settled to the bottom of the beaker. After being removed from the water bath, the beaker was allowed to cool to a moderate temperature. Filtration was used to obtain the particles. The filtered particles were baked for 18 hours at  $80^\circ C$  to dry them out. When the fine materials were finally produced, they were in powder form Cu K $\alpha$  radiation ( $\lambda = 1.5405 \text{ \AA}$ ) was used in the x-ray powder diffraction technique to characterise these materials. These prepared samples ( $x = 0.4$  and  $0.6$ ) compositions had their lattice parameter computed. The Debye-Scherrer formula was used to estimate the average crystallite size of each sample [18-20].

#### B. Ceramic method (Solid state method):

The synthesis of  $Mn_xZn_{(1-x)}Fe_2O_4$  by solid-state method involves the following steps which showed in Fig 2:

**Weighing and mixing:** Weigh the required amounts of high-purity  $MnO$ ,  $ZnO$ ,  $Fe_2O_3$ , and a suitable dispersant (e.g. polyvinyl alcohol). The powders are then mixed thoroughly in a ball mill or mortar and pestle to ensure a homogeneous mixture.

**Grinding and calcination:** The powder mixture is then ground to a fine powder and calcined in air at a temperature of  $800-1000^\circ C$  for 5 hours to obtain the desired spinel phase.

**Milling and pelletizing:** The calcined powder is then ground again to obtain a fine powder obtain a dense and homogeneous  $Mn_xZn_{(1-x)}Fe_2O_4$  ceramic.

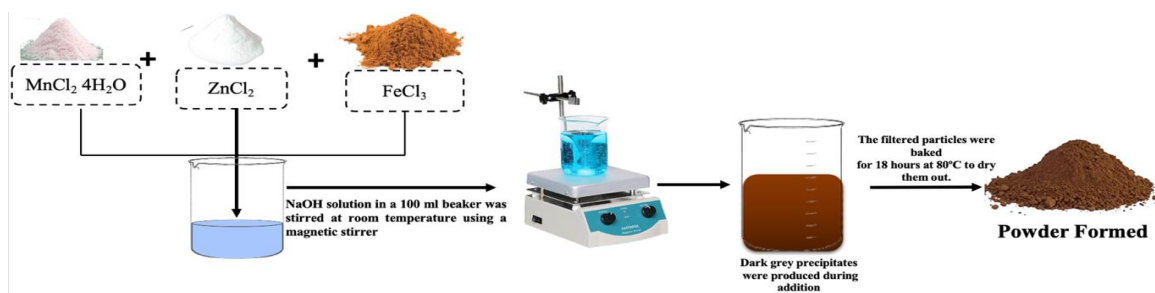


Fig.1. Schematic diagram of co-precipitation method.

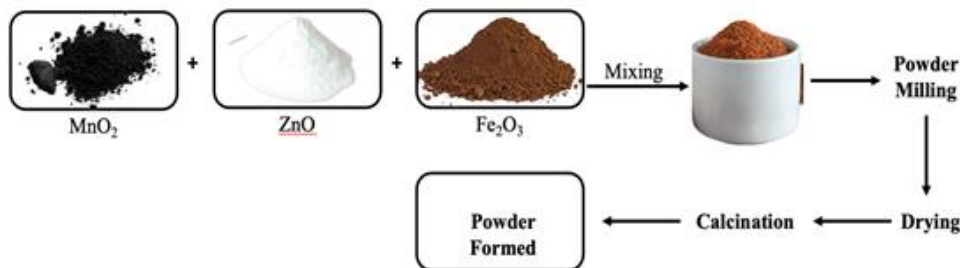


Fig. 2. Schematic diagram of Solid state method.

Characterization: The synthesized ceramic is characterized using techniques such as X-ray diffraction (XRD), scanning electron microscopy (SEM), and EDX analysis to determine its crystal structure, morphology and elemental composition [21,22].

Overall, the solid-state method is a simple and cost-effective method for synthesizing  $Mn_xZn_{1-x}Fe_2O_4$  ceramic with good magnetic properties. These samples of  $x = 0.4$  and  $0.6$  compositions had their lattice parameter computed. The Debye-Scherrer formula was used to estimate the average crystallite size of each sample [23].

## II. Results and discussion

### 2.1 X-ray diffraction analysis

The sample was investigated by using X-ray diffraction techniques. The powder X-ray diffraction method observed reflections between  $20^\circ$  and  $80^\circ$  angles. The Mn-Zn ferrite samples were synthesized by conventional solid-state, and the Co-precipitation methods prepared were examined. For all compositions of  $Mn_xZn_{1-x}Fe_2O_4$ , single-phase cubic spinel structure development is not shown in XRD patterns for all samples created by the ceramic technique but with some impurity peaks are observed its due to low sintering temperature and precursors used as started materials. Fig.3 displays the X-ray spectra of these materials (a and b). The development of ferrites is demonstrated by comparing Figures 3 (a) and 3(b) of the mixture's XRD pattern. As a result, it is discovered that the ceramic approach is not that much helpful in the synthesis of ferrites [24].

The co-precipitation method was used to manufacture samples of  $Mn_xZn_{1-x}Fe_2O_4$  with compositions ( $x=0.4$  &  $0.6$ ) and the X-ray diffraction spectra show that Mn-Zn ferrite formed as a single phase in each case. The patterns observed match the XRD patterns for Mn-Zn ferrite that have been described in the literature. Figures 3 (a) and 3(b)

depict the X-ray diffraction pattern for  $Mn_xZn_{1-x}Fe_2O_4$  ( $x=0.4, 0.6$ ) for the samples A1, A2, and S1, S2. The synthesized ferrite sample is supported by the diffraction lines. Wide lines show that the particles are nanoscale. The average particle size for each composition was calculated from the line width of a number of peaks using the Scherrer formula [22]. Table 1 lists the values for the particle size and lattice parameter derived from the X-ray data. The errors listed are the sizes' standard deviations from the mean value. The relative ionic radius can be used to explain why the lattice parameter increases with zinc concentration.  $Zn^{2+}$  ions have an ionic radius of  $0.82$ , which is less than  $Mn^{2+}$  ions' ionic radius of  $0.91$ . As the concentration of  $Zn^{2+}$  ions in the Mn-Zn ferrite increases (i.e.,  $x$  in  $Mn_xZn_{1-x}Fe_2O_4$  becomes larger), the average ionic radius of the A and B site metal ions in the crystal structure increases. This is because the ionic radius of Zn ( $0.74 \text{ \AA}$ ) is larger than that of Mn ( $0.83 \text{ \AA}$ ). When the size of the  $Zn^{2+}$  ions increases, the lattice parameter of the crystal also increases, since the larger ions require a larger lattice to maintain the same crystal structure. This is known as the "size effect" [25-27].

The Scherer formula was used to compute the lattice constants 'a' for samples generated using the two different procedures and the results were found to be in good agreement with the reported values. According to calculated lattice parameter values for the ferrite samples, the lattice constant value increased as the concentration ( $x$ ) of manganese increased (Table 1). For instance, the lattice constant for  $Mn_{0.4}Zn_{0.6}Fe_2O_4$  in the ceramic method progressively rises to  $8.44 \text{ \AA}$  for  $Mn_{0.6}Zn_{0.4}Fe_2O_4$ . Similar to this, the lattice constant "a" for  $Mn_{0.4}Zn_{0.6}Fe_2O_4$ , which is  $8.45 \text{ \AA}$ , climbs to  $8.46 \text{ \AA}$  for  $Mn_{0.6}Zn_{0.4}Fe_2O_4$  when using the wet chemical approach (Table 1). This increase may be a result of the  $Mn^{2+}$  and  $Zn^{2+}$  cations larger ionic radii. Larger  $Mn^{2+}$  cations ( $0.83 \text{ \AA}$ ) replace smaller  $Zn^{2+}$  cations ( $0.73 \text{ \AA}$ ) in the samples when  $Mn^{2+}$  concentration rises. In their investigation of Mn-Zn ferrites, various researchers

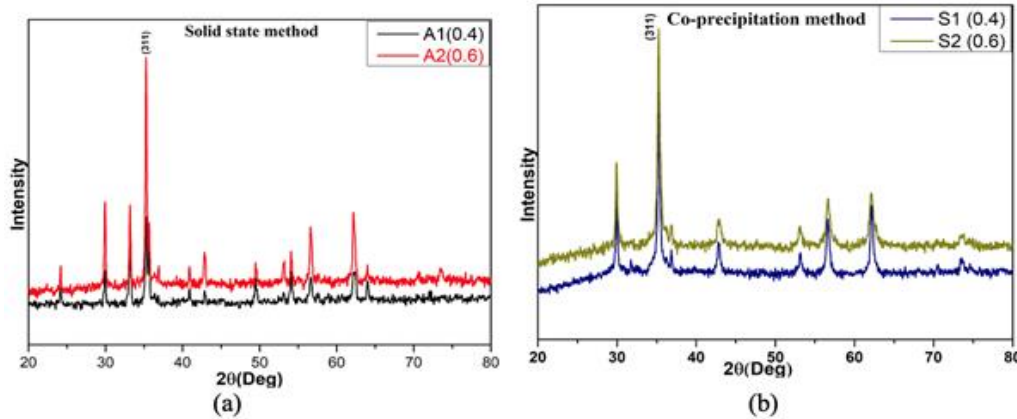


**Fig. 3.** The X-ray diffraction pattern for  $Mn_xZn_{1-x}Fe_2O_4$  ( $x = 0.4, 0.6$ ) prepared by ceramic method and co-precipitation method.

**Table 1.**

X	Composition	Ceramic method		Co-precipitation method	
		a in $\text{\AA}$ (a)	Crystallite size nm(b)	a in $\text{\AA}$ (b)	Crystallite size nm(b)
0.4	$Mn_{0.4}Zn_{0.6}Fe_2O_4$	8.44	27.40	8.46	29.76
0.6	$Mn_{0.6}Zn_{0.4}Fe_2O_4$	8.41	37.16	8.45	56.80

reported comparable observations.

**2.2 Scanning Electron Microscopic Analysis (SEM)**

The properties of ferrites are significantly influenced by the surface shape, grain size, and elemental makeup of the samples. More details on the grain nature of the samples are revealed by looking at the surface morphology and grain size variation of the system  $Mn_xZn_{1-x}Fe_2O_4$  ( $x=0.4$ ) with regard to Mn content. Figures 4.1–4.2 display typical micrographs for both series (A2 and S2) for the samples with  $x=0.4$  along with the accompanying EDX spectra. The results of the SEM analysis demonstrate the extreme homogeneity of all the samples and shows micro powder with bead like structure formation. Additionally, there are no secondary phases, as seen by the sharp SEM pictures of all the samples. The lack of extra peaks in the XRD patterns supports this. The lack of extra peaks in the XRD patterns supports this. All of the samples' micrographs demonstrate the presence of numerous smaller grains with numerous interfaces, which directly affect the properties of these ferrites [28].

Fig. 4.1 SEM images and EDAX Spectra of  $Mn_{0.4}Zn_{0.6}Fe_2O_4$  ( $x=0.4$ ) ferrite sample prepared by co-precipitation method

**2.3 EDAX Analysis**

EDX analysis was used to examine the compounds' semi-quantitative elemental makeup. In Figures 4.1 and 4.2, the EDX spectra of each sample are displayed (b). The spectra demonstrate that Zn, Mn, and Fe are present in the produced ferrite powders. There is a small variation in the samples compositions levels of Zn, Mn, and Fe, according to the analysis. The mutual quantitative ratio of the elements, however, shows that the composition of the synthesized materials is quite near to the one assumed. Possible Zn evaporation during the synthesis at high temperatures may be the cause of the small disproportions [29,30].

**Table 2.**

Mass contents of individual ions in Mn-Zn ferrites as determined from EDAX analysis

Element	A2(x = 0.4)		S2(x = 0.4)	
	Weight %	Atomic%	Weight%	Atomic %
O K	24.71	54.57	25.35	55.37
Mn L	12.06	7.76	12.54	7.98
Fe L	37.99	24.03	37.83	23.67
Zn L	25.24	13.64	24.28	12.98

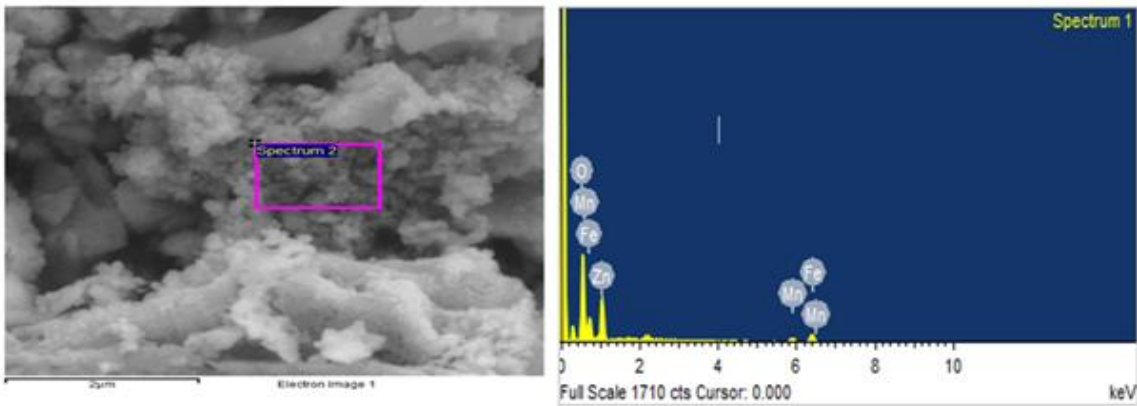


**Fig.4.1(a)**

**Fig.4.1(b)**

**Fig. 4.1.** SEM images and EDAX Spectra of  $Mn_{0.4}Zn_{0.6}Fe_2O_4$  ( $x = 0.4$ ) ferrite sample prepared by co-precipitation method.

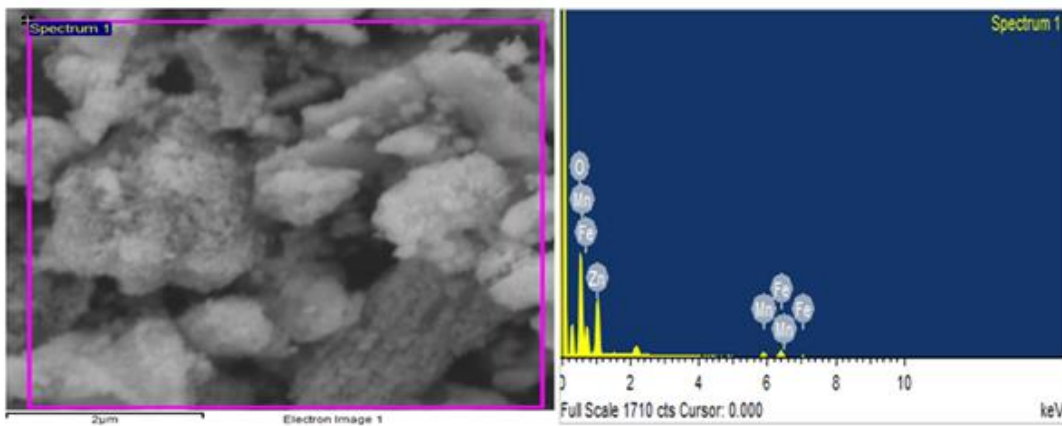


**Fig. 4.2 (a)**

**Fig.4.2 (b)**

**Fig. 4.2.** SEM images and EDAX Spectra of  $Mn_{0.4}Zn_{0.6}Fe_2O_4$  ( $x = 0.4$ ) ferrite sample prepared by ceramic method.

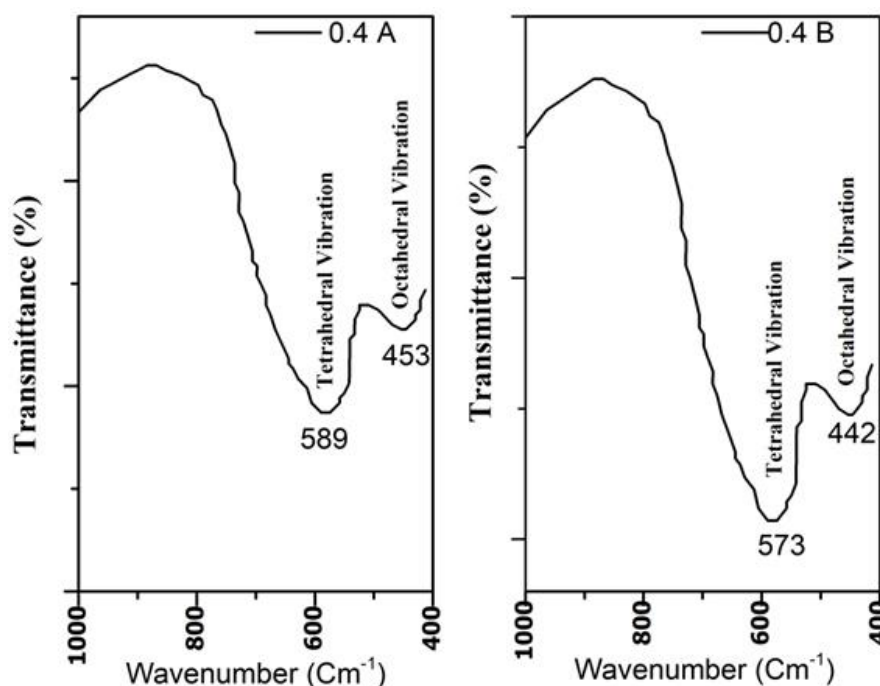


Fig.5. FTIR analysis of  $Mn_{0.4}Zn_{0.6}Fe_2O_4$  samples (A- Solid state, B- Co- ppt method).

#### 2.4 FTIR Analysis

Figure 5 demonstrates the FTIR spectra of the solid state (Fig. 5A) and chemical method (Fig.4B) samples ferrite samples with  $X = 0.4$  in the range from 400 to 1000  $cm^{-1}$ . The spectra show two main absorption bands below 600  $cm^{-1}$  which is a common characteristic of ferrites[30]. Metal- oxygen stretching vibrations both the samples confirms the cubic structure [31]. The high frequency band lies in the range 573–589  $cm^{-1}$  while the low frequency band lies in the range 442–453  $cm^{-1}$ . Normal ferrites both absorption bands depend on the nature of octahedral Me–O stretching (where Me-metal) vibration and nature of tetrahedral Me–O stretching vibration reveals formation ferrites [33,34]. These two observed bands ( $\nu_1$  and  $\nu_2$ ) correspond to the intrinsic vibrations of tetrahedral and octahedral  $Fe^{3+}-O^{2-}$  complexes, respectively. Thus FTIR confirms the cubic nature of ferrite samples [35].

## Conclusions

Cubic Spinel  $Mn_xZn_{1-x}Fe_2O_4$  ( $x=0.4$  &  $0.6$ ) particles

have been successfully prepared by both the co-precipitation process and the Solid state method. Samples examined using XRD, SEM and EDX consequences confirmation of formation of pure cubic-phase spinel-type by using Co-precipitation process  $Mn_xZn_{1-x}Fe_2O_4$  structure with well-crystalline nature by comparing both the synthesis methods Co-precipitation method is the best Mn-Zn synthesis. The average crystallite size was observed in the range from 27 to 37 nm for the ceramic method and 29 to 56 nm for Co-precipitation method. FTIR analysis showed for both synthesis method have absorption band in the range of 442–453  $cm^{-1}$  ( $\nu_1$ ) and 573–589  $cm^{-1}$  ( $\nu_2$ ). SEM images showed the ferrites samples particles-like morphology of the samples, shows micro powder with bead like structure formation. The quantitative mutual ratio of the elements (EDX) demonstrates that the composition of the synthesized materials.

**Pathan A. T.**–; Assistant Professor, Ph.D.;  
**Shaikh A. M.**–; Professor, Ph.D.;  
**Sushant S.K.** –; Assistant Professor, Ph.D.;  
**Shridhar N. Mathad** – Associate Professor, Ph.D.

- [1] K.P Mudholakar, S. Tambe Vinaykumar, S.S Kakati, S. N. Mathad., *Effect of Sintering condition on Magnetization and Microstructure of  $Cu_xCo_{(1-x)}Fe_2O_4$  Ferrites*, Int. J. Adv. Sci. Eng, 9(2), 2678 (2022); <https://doi.org/10.29294/IJASE.9.2.2022.2678-2685>.
- [2] R. S. Totagi, N. J. Choudhari, S. S. Kakati, C. S. Hiremath, S. B. Koujalagi, and R. B. Pujar, *Electrical properties of Ni-Mg-Cu nanoferrites synthesized by sucrose precursor technique*, Scholars Research Library Der Pharma Chemica, 7(3), 11(2015); Accessed: Feb. 21, 2023.
- [3] S. S. Gandhad, P. M. Patil, S. N. Mathad, L. v. Hublikar, P. R. Jeergal, and R. B. Pujar, *Effect of Aluminum Doping on Structural and Mechanical Properties of Ni–Mg Ferrites*, International Journal of Self-Propagating High-Temperature Synthesis, 28(4), 271 (2019); <https://doi.org/10.3103/S1061386219040046/FIGURES/3>.
- [4] A. Kumar, S. Molakeri, S. Kalyane, A. B. Kulkarni, and S. N. Mathad, *Elastic Properties of Nickel Ferrite Synthesized by Combustion and Microwave Method using FT-IR Spectra*, Int. J. Adv. Sci. Eng, 3(422), (2017), Accessed: Feb. 21, 2023.

- [5] M. R. Patil, M. K. Rendale, S. N. Mathad, and R. B. Pujar, *FTIR Spectra and Elastic Properties of Cd-Substituted Ni-Zn Ferrites I*, International Journal of Self-Propagating High-Temperature Synthesis, 26(1), 33 (2017); <https://doi.org/10.3103/S1061386217010083>.
- [6] S. S. Yattinahalli, S. B. Kapatkar, N. H. Ayachit, and S. N. Mathad, *Synthesis and structural characterization of nanosized nickel ferrite*, International Journal of Self-Propagating High-Temperature Synthesis, 22(3), 147 (2013); <https://doi.org/10.3103/S1061386213030114/METRICS>.
- [7] S. N. Adarakatti V S Pattar P K Korishettar, B V Grampurohit, S. N. Mathad. A B Kulkarni, *Synthesis, structural and electrical studies of li-ni-cu nano ferrites*, Acta Chemica Iasi, 26(1), 1 (2018); <https://doi.org/10.2478/achi-2018-0001>.
- [8] Shashidhargouda. H. R. and S. N. Mathad, *Synthesis and structural analysis of Ni<sub>0.45</sub> Cu<sub>0.55</sub> Mn<sub>2</sub>O<sub>4</sub> by Williamson–Hall and size–strain plot methods*, Ovidius University Annals of Chemistry, 29(2), 122 (2018); <https://doi.org/10.2478/AUOC-2018-0018>.
- [9] S. Vijaykumar, V. R. Hiremath, S. K. Sushant, and S. N. Mathad, *Synthesis, Characterization and Evaluation of  $\delta$ -Al<sub>2</sub>O<sub>3</sub> Nanoparticles Prepared by Chemical Method with Variation of pH*, Journal of Nano- and Electronic Physics, 14 (3), 3027 (2022); [https://doi.org/10.21272/JNEP.14\(3\).03027](https://doi.org/10.21272/JNEP.14(3).03027).
- [10] S. Kakati, M. K. Rendale, and S. N. Mathad, *Synthesis, Characterization, and Applications of CoFe<sub>2</sub>O<sub>4</sub> and M-CoFe<sub>2</sub>O<sub>4</sub> (M = Ni, Zn, Mg, Cd, Cu, RE) Ferrites: A Review*, International Journal of Self-Propagating High-Temperature Synthesis, 30(4), 189 (2021); <https://doi.org/10.3103/S1061386221040038>.
- [11] S. S. Yattinahalli, S. B. Kapatkar, and S. N. Mathad, *Review of Nanoscience Materials and its applications*, Research Journal of Engineering and Technology, 7(3), 121 (2016); <https://doi.org/10.5958/2321-581X.2016.00024.6>.
- [12] S. S. Yattinahalli, S. B. Kapatkar, and S. N. Mathad, *Structural and Mechanical Properties of a Nano Ferrite*, Advanced Science Focus, 2(1), 42(2014); <https://doi.org/10.1166/ASFO.2014.1079>.
- [13] A. B. Kulkarni and S. N. Mathad, *Effect of Sintering Temperature on Structural Properties of Cd doped Co-Zn Ferrite*, Journal of Nano- and Electronic Physics, 10(1), 1001 (2018); [https://doi.org/10.21272/JNEP.10\(1\).01001](https://doi.org/10.21272/JNEP.10(1).01001).
- [14] R. M. Shedam, A. M. Bagwan, S. N. Mathad, A. B. Gadkari, M. R. Shedam, and R. G. Sonkawade, *Nd<sup>3+</sup> added Mg–Cd ferrite material study the thick film gas sensing properties*, Mater Chem Phys, 293, 126871 (2023); <https://doi.org/10.1016/j.matchemphys.2022.126871>.
- [15] R. M. Shedam, P. P. Kashid, S. N. Mathad, R. B. Deshmukh, M. R. Shedam, and A. B. Gadkari, *Ferrites gas sensors: A Review*, Physics and Chemistry of Solid State, 23(3), 626 (2022); <https://doi.org/10.15330/PCSS.23.3.626-640>.
- [16] S. U. Durgadsimi, V. R. Kattimani, N. S. Maruti, A. B. Kulkarni, and S. N. Mathad, *Synthesis and structural analysis of nickel ferrite synthesized by co-deposition*, Eurasian Physical Technical Journal, 18(4) (38), 14-19 (2021); <https://doi.org/10.31489/2021NO4/14-19>.
- [17] R. Y. Kolekar, S. B. Kapatkar, and S. N. Mathad, *Nickel-Doped Cobalt Zinc Ferrites Co<sub>0.8-x</sub>Ni<sub>x</sub>Zn<sub>0.2</sub>Fe<sub>2</sub>O<sub>4</sub>(x=0.0–0.56) by Solid-State Reaction: Synthesis and Characterization*, International Journal of Self-Propagating High-Temperature Synthesis, 29(4), 196 (2020); <https://doi.org/10.3103/S1061386220040044/FIGURES/5>.
- [18] R. Vishwarup and S. N. Mathad, *Facile Synthesis of Nano Mg-Co Ferrites (x=0.15, 0.20, 0.25, 0.30, 0.35, and 0.40) via Co-precipitation Route: Structural Characterization*, Materials International, 2(4) 0471-0476 (2020); <https://doi.org/10.33263/Materials24.471476>.
- [19] M. B. Tahir, T. Iqbal, A. Hassan, and S. Ghazal, *Wet Chemical Co-precipitation Synthesis of Nickel Ferrite Nanoparticles and Their Characterization*, J InorgOrganometPolym Mater, 27(5), 1430 (2017); <https://doi.org/10.1007/S10904-017-0598-5/FIGURES/7>.
- [20] P. Zsabka, G. Leinders, A. Baena, T. Cardinaels, K. Binnemans, and M. Verwerft, *Synthesis of gadolinium-doped thorium dioxide via a wet chemical route: Limitations of the co-precipitation method*, Journal of Nuclear Materials, 489, 211 (2017); <https://doi.org/10.1016/J.JNUCMAT.2017.03.052>.
- [21] Z. Zhang, Y. Liu, G. Yao, G. Zu, and Y. Hao, *Synthesis and Characterization of NiFe<sub>2</sub>O<sub>4</sub> Nanoparticles via Solid-State Reaction*, Int J Appl Ceram Technol, 10(1), 142 (2013); <https://doi.org/10.1111/J.1744-7402.2011.02719.X>.
- [22] P. Parhi, T. N. Karthik, and V. Manivannan, *Synthesis and characterization of metal tungstates by novel solid-state metathetic approach*, J Alloys Compd, 465(1-2), 380 (2008); <https://doi.org/10.1016/J.JALLCOM.2007.10.089>.
- [23] S. Mathad, *Solid-State Synthesis and Structural Features of Li<sub>0.5</sub>Ni<sub>0.75-x/2</sub>Zn<sub>x/2</sub>Fe<sub>2</sub>O<sub>4</sub> Ferrites*, International Journal of Self-Propagating High-Temperature Synthesis, (2019); <https://doi.org/10.3103/S1061386219010060>.
- [24] J. F. Marco, J. R. Gancedo, M. Gracia, J. L. Gautier, E. Ríos, and F. J. Berry, *Characterization of the Nickel Cobaltite, NiCo<sub>2</sub>O<sub>4</sub>, Prepared by Several Methods: An XRD, XANES, EXAFS, and XPS Study*, J Solid State Chem, 153(1), 74 (2000); <https://doi.org/10.1006/JSSC.2000.8749>.
- [25] S. S. Kakati, T. M. Makandar, M. K. Rendale, and S. N. Mathad, *Green Synthesis Approach for Nanosized Cobalt Doped Mg–Zn through Citrus Lemon Mediated Sol–Gel Auto Combustion Method*, International Journal of Self-Propagating High-Temperature Synthesis, 31(3), 131 (2022); <https://doi.org/10.3103/S1061386222030049/TABLES/2>.

- [26] S. Kazi, S. Feeda. S. S. Kakati, S. N. Mathad, S. L. Galgali, M. K. Rendale, *Sintering Temperature Dependent Structural and Mechanical Studies of  $Ba_xPb_{1-x}TiO_3$  Ferroelectrics*, Journal of Nano- and Electronic Physics, 12(4), 4018 (2020); [https://doi.org/10.21272/JNEP.12\(4\).04018](https://doi.org/10.21272/JNEP.12(4).04018).
- [27] M. C. Dimri, S. C. Kashyap, D. C. Dube, and S. K. Mohanta, *Complex permittivity and permeability of Co-substituted NiCuZn ferrite at rf and microwave frequencies*, J. Electroceram., 16(4), 331 (2006); <https://doi.org/10.1007/s10832-006-9874-4>.
- [28] R. Sen, P. Jain, R. Patidar, S. Srivastava, *Synthesis and characterization of nickel ferrite ( $NiFe_2O_4$ ) nanoparticles prepared by sol-gel method*, Elsevier, 2, 3750 (2015); <https://doi.org/10.1016/j.matpr.2015.07.165>.
- [29] G. Padmapriya, A. Manikandan, V. Krishnasamy, S. K. Jaganathan, and S. A. Antony, *Enhanced Catalytic Activity and Magnetic Properties of Spinel  $Mn_xZn_{1-x}Fe_2O_4$  ( $0.0 \leq x \leq 1.0$ ) Nano-Photocatalysts by Microwave Irradiation Route*, J Supercond Nov Magn, 29 (8), 2141 (2016); <https://doi.org/10.1007/S10948-016-3527-X>.
- [30] L. C. Shidaganal, A. B. Kulkarni, S. B. Kapatkar, S. N. Mathad, and R. B. Pujar, *Al-Doped Co-Cd Nanoferrites by Solution-Combustion Synthesis: Preparation and Structural Characterization*, International Journal of Self-Propagating High-Temperature Synthesis, 29(3), 176 (2020); <https://doi.org/10.3103/S1061386220030103>.
- [31] R. D. Waldron, *Infrared spectra of ferrites*, Physical Review, 99(6), 1727(1955); <https://doi.org/10.1103/PHYSREV.99.1727>.
- [32] M. K. Rendale, S. N. Mathad, and V. Puri, *Structural, mechanical and elastic properties of  $Ni_{0.7-x}Co_xZn_{0.3}Fe_2O_4$  nano-ferrite thick films*, Microelectronics International, 34(2), 57 (2017); <https://doi.org/10.1108/MI-02-2016-0009/FULL/HTML>.
- [33] S. L. Galagali et al., *Fourier transform infrared spectroscopy and elastic properties of  $Mg_{1-x}Cd_xFe_2O_4$  ferrite systems.*, Thaiscience.info, 41(5), 992 (2023).
- [34] M. Patil, M. Rendale, S. Mathad, FTIR spectra and elastic properties of Cd-substituted Ni-Zn ferrites, International Journal of Self-Propagating High-Temperature Synthesis, 26(1), 33 (2017); <https://doi.org/10.3103/S1061386217010083>.
- [35] Ied Mohammed Mnawe , M. Y. Hassaan , Osama Mohmaed Hameda , A.S. Abdel-Moety, *XRD, FTIR and electrical properties investigation of  $Ni_{0.6}Zn_{0.4}Cr_xFe_{2-x}O_4$  thin films*, NVEO, 9(1), 1617 (2022).

A.T. Патан<sup>1</sup>, А.М.Шейх<sup>2</sup>, С.К. Сушант<sup>3</sup>, С.Н. Матхад<sup>3</sup>

## Вплив методів синтезу та порівняльне дослідження структурних властивостей мікро- та наноферитів

<sup>1</sup>Кафедра фізики, Інженерний коледж Сабу Сіддіка, Мумбаї, 400008, Індія, [asrar.pathan@rediffmail.com](mailto:asrar.pathan@rediffmail.com),

<sup>2</sup>Кафедра електроніки, Новий коледж, Колхатур, 416014, Індія,

<sup>3</sup>Кафедра інженерної фізики, К.Л.Е. Технологічний інститут, Хаббали, 580027 Карнатака, Індія

Зразки фериту  $Mn_{(x)}Zn_{(1-x)}Fe_2O_4$  із  $x = 0,4$  та  $0,6$  синтезовано твердотільним методом і методом співосадження. Щоб визначити вплив різних концентрацій ( $x$ ) на структуру фериту, розмір частинок і кристалічні фази, підготовлені зразки аналізували за допомогою рентгенівської дифракції (XRD). Рентгенограми показали, що синтезовані зразки мають однофазну структуру кубічної шпінелі. Аналіз FTIR показав, що для обох методів синтезу характерною є смуга поглинання в діапазоні від 400 до 1000  $cm^{-1}$ . Аналіз SEM показує надзвичайну однорідність усіх зразків. Для дослідження  $Mn_{0,4}Zn_{0,6}Fe_2O_4$  використовували EDX аналіз. Приготовані феритові порошки містять Mn, Zn і Fe, як було показано в обох методах синтезу. У цьому дослідженні пропонуються альтернативні шляхи синтезу цих феритів, щоб обійти деякі обмеження традиційного методу приготування.

**Ключові слова:** ферити, XRD, твердотільний метод синтезу, метод співосадження.